Axial and angular correlations between colloidal particles in narrow cylindrical pores

M. Chávez-Páez and M. Medina-Noyola
Instituto de Física, Universidad Autónoma de San Luis Potosí, Alvaro Obregón 64, 78000 San Luis Potosí, SLP, Mexico

M. Valdez-Covarrubias
Departamento de Física, Universidad de Sonora, Apartado Postal 1626, 83000 Hermosillo, Sonora, Mexico
(Received 26 October 1998; revised manuscript received 10 December 1999)

In this work we present a study of the local structure of a model colloidal suspension highly confined inside a cylindrical pore. Such a study is based in Monte Carlo computer simulations, using the repulsive part of the Derjaguin-Landau-Verwey-Overbeek potential as the pair interaction between particles. The structural properties calculated here are the concentration profile $n(\rho)$, the axial pair correlation function $g(z)$, and the axial-angular pair correlation function $g(z,\varphi)$. The behavior of these quantities is analyzed as a function of the density of colloidal particles in the restricted space, and as a function of the size of the pore.

PACS number(s): 82.70.Dd, 05.40.−a

I. INTRODUCTION

When a colloidal suspension is under the influence of an external field the local density of particles, uniform in the absence of the field, varies from point to point in space [1]. The external field can be gravity, an electrical field applied on a charged system, or even a wall that confines the suspension within a given region of space. In the last few years, theoretical and experimental work has been carried out in this class of systems [2,3]. On the experimental side, by using optical techniques such as laser trapping and videomicroscopy, the effective two-dimensional (2D) static structure and the effective 2D interaction potential of colloidal particles confined between two glass plates have been measured [3]. On the theoretical side, employing theoretical schemes, mainly borrowed from the theory of simple liquids, and at the Derjaguin-Landau-Verwey-Overbeek (DLVO) level of description for the pair potential between particles [4,5], the concentration profile of colloidal suspensions in front of a wall, or confined in a slit pore, has been calculated and compared with simulation results [2]. At this same level of description the equilibrium structure of a colloidal suspension confined inside a cylindrical pore has also been studied [6,7] in terms of the local concentration profile of the particles.

In the present work we will be concerned with the same system, namely, a colloidal suspension confined in a cylindrical pore, but here we study the structure of the suspension in terms of the pair correlations between the particles, and not only of the wall-particle correlations (i.e., the concentration profiles). In particular, we will be interested in the pair correlations along the axis, and also in the angular pair correlations when the colloidal suspension is under severe confinement, for which we will employ a standard Monte Carlo (MC) simulation technique [8].

As in previous work [6], the system we have in mind consists of colloidal particles of charge Q suspended in a polar solvent, and confined in the interior of a very long cylindrical capillary with surface charge σ_c. Following Ref. [6] we will base our study on the DLVO level of description for the particle-particle interaction, and for the wall-particle interaction. Thus, we shall model the interaction potential between two particles, $u(r)$, as the repulsive part of the DLVO potential, i.e.,

$$\beta u(r)=\beta u_{\mathrm{HS}}(r)+A_p\frac{\exp[-z_D(r/\sigma-1)]}{(r/\sigma)}, \qquad (1.1)$$

where $u_{\mathrm{HS}}(r)$ is the hard-sphere potential, $\beta^{-1}=k_BT$, with k_B being Boltzmann's constant and T the temperature, and $z_D\equiv\kappa\sigma$ with κ being the inverse Debye length and σ the diameter of the particles. A_p is, in units of k_BT, the potential energy of two particles at contact. As for the wall-particle potential $\Psi(\mathbf{r})$, we will use

$$\beta\Psi(\rho)=A_w\frac{I_0(\kappa\rho)}{I_0(\kappa R')-1}, \quad \rho<R', \qquad (1.2)$$

with ρ being the distance from position $\mathbf{r}$ to the cylinder's axis. This form of the potential derives from solving the linearized Poisson-Boltzmann equation for an electrolyte confined inside the charged cylinder. In this equation $I_0(x)$ is the zeroth-order modified Bessel function, and R' is the distance from the cylinder axis to the point at which a particle is in contact with the cylinder's inner hard wall. Thus, if R is the actual radius of the cylinder, then $R'\equiv R-\sigma/2$. In units of k_BT, we have that A_w in Eq. (1.2) is the electrostatic potential of a particle in contact with the cylinder wall, referred to the potential at the center of the cylinder.

II. STRUCTURE AND SIMULATION DETAILS

In this work we perform Monte Carlo simulations in the *NVT* ensemble [8]. To do this, we build a cylindrical simulation box whose length is calculated through the relation $L=N[\pi R^2 n_c]^{-1}$, where N is the number of particles used in the simulation runs, R is the radius of the cylinder, and n_c is the number density of particles in the cylinder. In this way, the volume of the basic simulation box is $V=\pi R^2 L$. In order to minimize edge effects due to the finite size of the simulation box, conventional periodic boundary conditions in the z direction have been used [8]. Once the interaction potentials have been given, the N particles are first randomly placed in

the simulation cell, and then are allowed to move according to the Monte Carlo scheme, until equilibrium is reached. Our criterion for the equilibrium is the stabilization of the fluctuations of the potential energy. Once equilibrium is reached, further configurations are generated in order to calculate the properties of interest.

The basic structure of the colloidal suspension inside the cylinder is given by the one-particle correlation function $n(\mathbf{r})$ (the concentration profile) and by the two-particle distribution function $n^{(2)}(\mathbf{r},\mathbf{r}')$ [9]. Due to the symmetry of the system the concentration profile becomes a function of the distance to the cylinder's axis, i.e., $n(\mathbf{r})=n(\rho)$. In order to calculate the simulated $n(\rho)$ we divide the simulation box in concentric cylindrical shells of length L, radius ρ, and width $\Delta\rho$. We then count the number of particles $N(\rho)$ within the volume $\Delta V=\pi[(\rho+\Delta\rho)^2-\rho^2]L$, and then compute the average

$$n(\rho)=\left\langle \frac{N(\rho)}{\Delta V}\right\rangle_{\text{conf}}, \tag{2.1}$$

where the angle brackets $\langle\rangle_{\text{conf}}$ indicate an average over many simulated configurations.

On the other hand, the inhomogeneous pair correlation function $g^{(2)}(\mathbf{r},\mathbf{r}')\equiv n^{(2)}(\mathbf{r},\mathbf{r}')[n(\mathbf{r})n(\mathbf{r}')]^{-1}$ is a more difficult quantity to calculate in the simulations. Instead of working with the full pair correlation function we will work with contracted versions of this function. The key to the appropriate definition of these correlation functions is the exact normalization condition [9]

$$\begin{aligned} N_b(N_b-1)&=\int\int n^{(2)}(\mathbf{r}_1,\mathbf{r}_2)d\mathbf{r}_1d\mathbf{r}_2\\ &=\int\int g^{(2)}(\mathbf{r}_1,\mathbf{r}_2)n(\mathbf{r}_1)n(\mathbf{r}_2)d\mathbf{r}_1d\mathbf{r}_2, \end{aligned} \tag{2.2}$$

where N_b is the number of particles in the volume V_b. By applying this later equation to our simulation box we see that it is possible to define the function

$$\begin{aligned} n(z,\varphi)&\equiv\frac{1}{N}\int g^{(2)}(\mathbf{r}_1,\mathbf{r}_2)n(\rho_1)n(\rho_2)\rho_1\rho_2d\rho_1d\rho_2dz_1d\varphi_1\\ &=\left(\frac{2\pi L}{N}\right)\int g^{(2)}(\rho_1,\rho_2,z,\varphi)n(\rho_1)n(\rho_2)\\ &\quad\times\rho_1\rho_2d\rho_1d\rho_2, \end{aligned} \tag{2.3}$$

where we have used the fact that, due to the symmetry of the system, the function $g^{(2)}(\mathbf{r}_1,\mathbf{r}_2)$ can be written as $g^{(2)}(\rho_1,\rho_2,z,\varphi)$, with $z=z_2-z_1$ and $\varphi=\varphi_2-\varphi_1$. From its definition, $n(z,\varphi)$ is the mean particle density in the volume element (a disk) delimited by the surfaces z and $z+dz$, and by the surfaces φ and $\varphi+d\varphi$, all these four surfaces measured from a particle that it is located at the point $(z=0,\varphi=0)$. The function $n(z,\varphi)$ defined through Eq. (2.3) satisfies the condition $n(z\to\infty,\varphi)=N/2\pi L$. This limiting condition allows us to define the function

$$\begin{aligned} g(z,\varphi)&=n_\varphi^{-1}n(z,\varphi)\\ &=n_\varphi^{-2}\int g^{(2)}(\rho_1,\rho_2,z,\varphi)n(\rho_1)n(\rho_2)\rho_1\rho_2d\rho_1d\rho_2 \end{aligned} \tag{2.4}$$

(with $n_\varphi\equiv N/2\pi L$), which satisfies the normalization condition

$$\int n_\varphi g(z,\varphi)dzd\varphi=N-1. \tag{2.5}$$

Equation (2.5) is equivalent to the normalization condition that the well-known radial distribution function satisfies for an homogeneous simple fluid [9]. In fact, from Eq. (2.5) we see that $g(z,\varphi)$ is the factor that modulates n_φ to give the local density $n(z,\varphi)$ in the volume element around the point (z,φ). Thus, $g(z,\varphi)$ determines the pair angular correlations along the axis of the cylinder.

In its turn, $g(z,\varphi)$ also allows the definition of another pair correlation function, namely, the axial pair correlation function, $g(z)$, through the relation

$$g(z)=\frac{1}{2\pi}\int g(z,\varphi)d\varphi=\frac{L}{N}\int n(z,\varphi)d\varphi, \tag{2.6}$$

which satisfies

$$\int n_\lambda g(z)dz=N-1, \tag{2.7}$$

where $n_\lambda=N/L$ is the number of particles per unit length, i.e., the lineal mean number density. As we see from Eq. (2.7), $g(z)$ determines the pair correlations along the axis of the cylinder.

The determination of these correlation functions in the simulations is based on the definitions above. Operationally, the axial pair correlation function $g(z)$ is defined through the relation

$$g(z)=\left\langle \frac{N(z)}{n_c\Delta V}\right\rangle_{\text{conf}}, \tag{2.8}$$

where $\Delta V=\pi R^2\Delta z$. Here $N(z)$ is the number of particles inside a disk of radius R and width Δz, located at a distance z from the central particle which is located at $(\rho_0,z_0=0,\varphi_0=0)$, i.e., the origin of coordinates is located in the center of the cylinder in such a way that the reference particle is located along the x axis, and in the plane $z=0$, regardless of its distance ρ_0 to the axis. From its definition, $g(z)$ gives information of the ordering along the z axis.

On the other hand, the axial-angular correlation function $g(z,\varphi)$ can be determined through the relation

$$g(z,\varphi)=\left\langle \frac{N(z,\varphi)}{n_c\Delta V}\right\rangle_{\text{conf}}, \tag{2.9}$$

where $\Delta V=(R^2/2)\Delta z\Delta\varphi$, and $N(z,\varphi)$ is the number of particles laying in the region between z and $z+\Delta z$, and forming an angle between φ and $\varphi+\Delta\varphi$ with the central particle located at the point $(\rho_0,z_0=0,\varphi=0)$. The function thus de-

fined gives information on the angular order between the particles and on how this order changes along the axis of the cylinder.

III. RESULTS

As it was mentioned before, our system consists of a model colloidal suspension confined in the interior of a cylinder, and the particle-particle and wall-particle interactions are given by Eqs. (1.1) and (1.2). In this work we will focus on the evolution of the structure of the particles as a function of n_c and of the size of the cylinder R. This means that we will fix all the other parameters defining the system, and will keep track of the structure as we let both n_c and R to vary. The values of the parameters we will keep fixed are $A_p = 400$, $A_w = 400$, and $z_D = 0.15$. For the simulation runs we use $N = 200$ particles. In every run the initial configuration was set to equilibrate over 10 000 Monte Carlo N cycles (in the basic MC cycle, a particle is selected randomly for displacement; an N cycle consists of N basic MC cycles), and 150 000 further N cycles were generated for the statistical averages. For the averages, we took the configurations generated after every N cycle.

A. Concentration profiles

Let us first present the corresponding results for $n^*(\rho) = n(\rho)\sigma^3$ as we vary the mean number density of particles inside the cylinder and the size of the cylinder. The first process can be achieved by externally compressing the colloidal suspension, or if we imagine that the cylinder is connected to a reservoir with bulk density n_b, by increasing n_b. The other process can be achieved by connecting cylinders of different sizes to the reservoir.

Figure 1 is a sequence in which we illustrate the behavior of the concentration profile as a function of $n_c^* \equiv n_c\sigma^3$ and R. In each figure the number density n_c^* takes the values $n_c^* = 3\times10^{-4}$, $n_c^* = 6\times10^{-4}$, $n_c^* = 6\times10^{-4}$, whereas R takes the values $R = 30\sigma$, $R = 20\sigma$, and $R = 10\sigma$. Let us discuss briefly the features of $n^*(\rho)$ appearing in this figure.

Figure 1(a) corresponds to $R = 30\sigma$. Here we see that, as a result of increasing n_c^*, the main peak of $n^*(\rho)$ is displaced towards the wall, whereas the height of the peaks increases. Since the height of the curves indicates how concentrated is the system in a given point, it is readily seen that the particles are structured in layers, which is one of the most interesting features of the concentration profiles. It is also evident that this layering structure is emphasized as the particle density increases since the height of the peaks become higher. These effects are the result of the equilibrium of two opposite trends, one which tends to confine the particles to the center of the cylinder and that is due to the interaction with the wall, and another in which the particles tend to occupy as much space as possible as a result of the repulsive interactions between them. This tendency towards expansion is higher as n_c^* increases, since the mean distance between particles is reduced.

The effects on the concentration profile due to the reduction of the available space is illustrated in Fig. 1(b). In this case $R = 20\sigma$ and the rest of the parameters were kept constant. From this figure we see that the different concentration

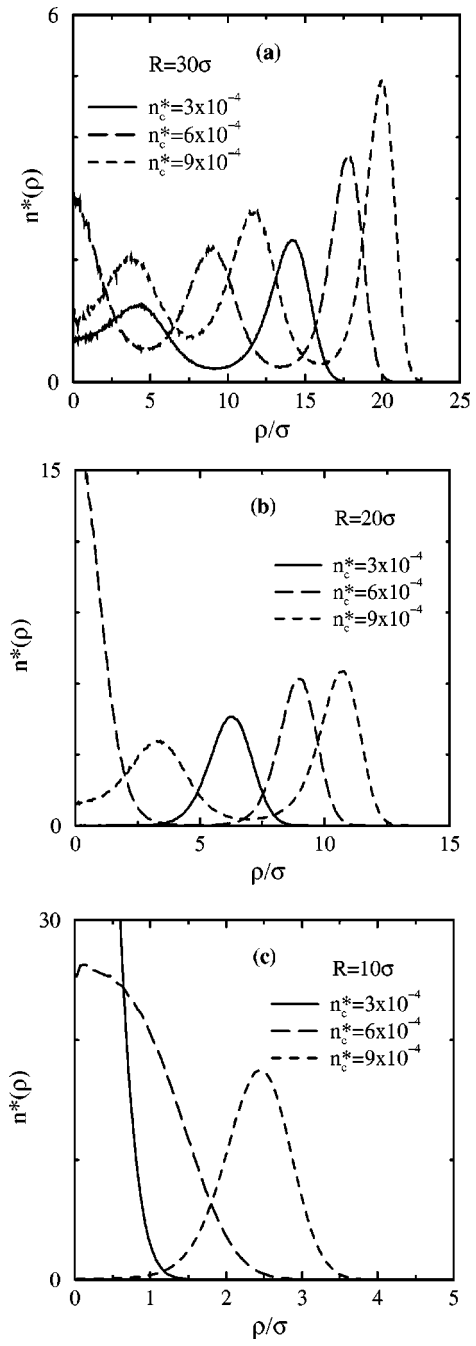

FIG. 1. Reduced concentration profiles $n^*(\rho) = n(\rho)\sigma^3$ ($\times10^3$) for a system with parameters $A_p = 400$, $A_w = 400$, $z_D = 0.15$. (a) $R = 30\sigma$; (b) $R = 20\sigma$; (c) $R = 10\sigma$.

profiles have fewer peaks, compared with the case $R = 30\sigma$, although the height of the different peaks is much higher, which means that the layering structure is much more pronounced in this case. It is interesting to see that the concentration profile for $n_c^* = 6\times10^{-4}$ consists of two disconnected regions, one high single peak at the center of the cylinder and one single peak located at $\rho \approx 8.5\sigma$, leaving a gap in the region $4\sigma < \rho < 6\sigma$. In the central peak the particles are arranged along the axis, with little space on the radial direction, whereas the particles in the other peak are arranged in such a way that they form a cylindrical shell of width $\Delta\rho \approx 2.5\sigma$, and centered at $\rho \approx 8.5\sigma$. On the other hand, the curve corresponding $n_c^* = 3\times10^{-4}$, earlier consisting of a

two-peak structure, now has one single peak. In this case, particles only arrange themselves in a cylindrical shell of width $\Delta\rho \approx 2\sigma$, centered at $\rho \approx 7\sigma$.

By further reducing the size of the pore we see that the trends just discussed are emphasized. Figure 1(c) presents the concentration profiles for the case $R=10\sigma$. In this case we see that the concentration profiles consist of a single peak for all the three values of n_c^* used here. In this case, however, the particles of the suspension are highly confined since the gap between the particles and the wall is about 6σ, i.e., more than half of the cylinder radius. The figure shows that $n^*(\rho)$ changes from a two-peak structure in Fig. 1(b), to a one-peak structure in the current figure for the case $n_c^* = 9\times10^{-4}$. On the other hand, the structure for $n_c^* = 3 \times 10^{-4}$ and $n_c^* = 6\times10^{-4}$ consists of a single peak at the center of the cylinder, sharper for $n_c^* = 3\times10^{-4}$ than for $n_c^* = 6\times10^{-4}$. As we will see later, the confinement of the particles into self-confined structures has important effects on the correlations between particles.

B. Axial pair correlations

In Sec. III A the main features of the concentration profile were shown. However, $n(\rho)$ comes from the average of the positions of the particles without taking into account their relative order. Thus, it only gives information of the average local density of particles as a function of the distance ρ from the center of the cylinder. In order to get more information about the three-dimensional (3D) ordering between the particles we now present our results for the axial pair correlation function, $g(z)$, for the cases presented in Fig. 1.

In Fig. 2(a) we plot our simulation results for the function $g(z)$ corresponding to the cases considered in Fig. 1(a). In this figure we see that $g(z)$ has a large, finite value at $z=0$, which indicates that every particle has a large probability of finding another particle in its same plane. This is possible since the particles are distributed over a broad space in the radial direction, such that there is not an effective volume exclusion effect between the particles in the z direction. On the other hand, we see that the oscillations of $g(z)$ are rather small, indicating that the particles are quite uniformly distributed around the central particle, i.e., the axial pair correlations are rather weak. However, we notice that such correlations are stronger as the value of the density decreases. This might seem contradictory since at larger densities the correlations should be stronger. This is true, however, for the full pair correlation function $g(r)$ in an homogeneous system, but not necessarily for partial pair correlation functions, such as $g(z)$, in an inhomogeneous system. In inhomogeneous systems, the competition between the pair potentials and the external field might yield the correlations to increase in a given spatial direction, whereas decreasing in others. In the present case we have that the particles are more confined for lower values of n_c^*, which emphasizes the pair interactions along the axis and leads to stronger correlations in this direction.

For the highest concentration plotted in Fig. 1(a), on the other hand, the outermost maximum of $n(\rho)$ corresponds to the cylindrical shell of largest radius, and hence, of largest volume. In fact, it also contains most of the particles, which tend to occupy uniformly all the volume of this shell. This

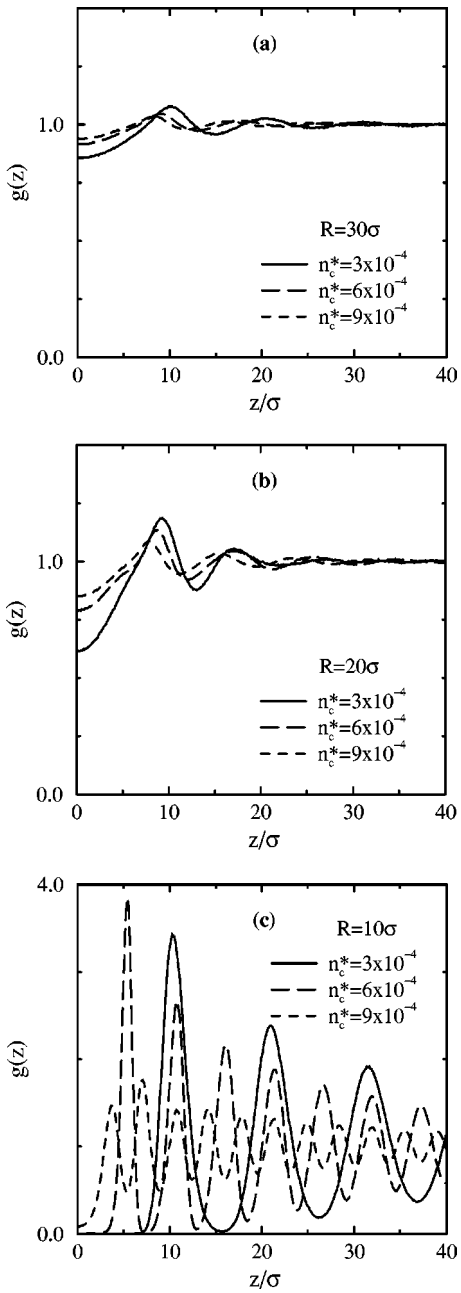

FIG. 2. Axial correlation functions corresponding to the systems in Fig. 1. (a) $R=30\sigma$; (b) $R=20\sigma$; (c) $R=10\sigma$.

allows the possibility that several particles occupy the same axial position (at different angles φ), and this leads to a weakening of the axial correlations. In order to check this, we calculated the axial correlations only among the particles located within the outermost shell. The resulting $g(z)$ happened to be virtually indistiguishable from the overall axial correlation function plotted in Fig. 2(a). This means that indeed, the axial structure is strongly dominated by the outermost shell. Thus, even if the axial correlations within the inner shells were stronger or dramatically different from those of this dominant shell, their contribution to the total $g(z)$ is actually very small, due to the overwhelming weight of the latter. However, we also calculated the axial correlations within the inner shells, and we found that these correlations are in fact different, but not dramatically, and not stronger, than those in the outermost shell.

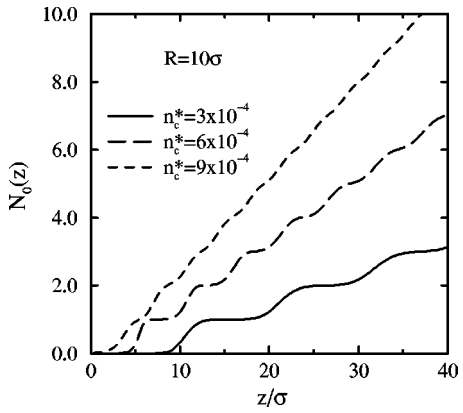

FIG. 3. Accumulated number of particles along the axis for the systems corresponding to Fig. 2(c); i.e., for the case $R=10\sigma$ in Fig. 2.

The results plotted in Fig. 2(b) indicate that the trends are similar for the case $R=20\sigma$. In this later case we see that the reduction of the space only slightly emphasizes the correlation between the particles.

In Fig. 2(c) we present the results for the axial correlations for a highly confined system, i.e., $R=10\sigma$. Here we see that the axial correlations between the particles are much stronger than in the previous cases. In fact, the curves corresponding to $n_c^*=3\times10^{-4}$ and $n_c^*=6\times10^{-4}$ resemble very much crystal-like structures. For these curves, the peaks are very high and the minima, at least the first two, virtually reach zero. Recalling that the concentration profiles for these two cases are single peaks in the center of the cylinder, we conclude that the axial correlations correspond mostly to pair correlations of effectively one-dimensional systems. This is not strictly true, since the broadness of the concentration profiles is finite. It is clear, however, that the 1D behavior predominates over such fluctuations. This idea is supported by the results plotted in Fig. 3, where we present the accumulated number of particles along the z axis, $N_0(z)$, which is calculated through the relation $N_0(z)=\int_0^z n_\lambda g(z_0)dz_0$. From this figure we see that the number of particles, under each peak of $g(z)$, is approximately one.

Going back to Fig. 2(c), it is interesting to notice that by increasing the density from $n_c^*=3\times10^{-4}$ to $n_c^*=6\times10^{-4}$ the peak of the concentration profile only increases its broadness by about 1σ, whereas the first peak of $g(z)$ shifts to the left by about 6σ. This indicates that basically the system is being compressed in the z direction, and that the radial structure is mainly dominated by the wall-particle interactions. Another interesting feature in this figure is the fact that the crystal-like structure disappears under a further increase of the density (for instance, $n_c^*=9\times10^{-4}$ in the figure). By looking at its concentration profile [see Fig. 1(c)] we see that the density is so high in this case that the particles have to accommodate in a cylindrical shell, allowing their mean distance along the axis to be reduced.

In addition to the features already shown, it is interesting to notice the virtual coincidence of the location of the *first* peak of $g(z)$ corresponding to the concentration $n_c^*=3\times10^{-4}$ with the location of the *second* peak for $n_c^*=6\times10^{-4}$, and with the location of the *third* peak for $n_c^*=9\times10^{-4}$. This coincidence repeats again for the second, fourth, and sixth peaks of, respectively, the same concentrations. This is another evidence of the essentially one-dimensional character of the distribution of particles inside very narrow cylinders. Under such conditions, the mean particle distance, which is also the distance between peaks in $g(z)$, is given by $1/\pi R^2 n_c$. Thus, the location of the i*th* peak of a given concentration n_c, is $z_i(n_c)=i/\pi R^2 n_c$, and hence, the ith peak of concentration n_1 will coincide with the jth peak of concentration n_2 if $i/j=n_1/n_2$, as it is the case for the peaks and concentrations referred to above.

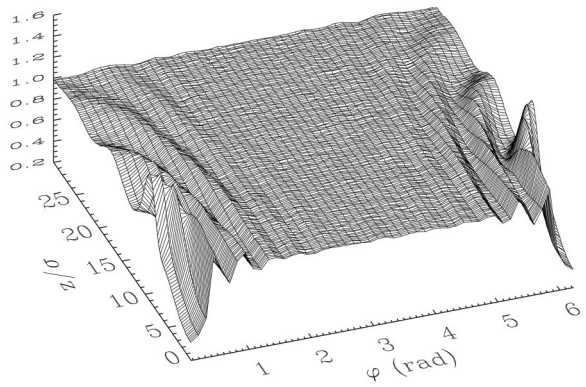

FIG. 4. Axial-angular pair correlation function for the parameters $A_p=400$, $A_w=400$, $z_D=0.15$, $R=30\sigma$, and $n_c^*=9\times10^{-4}$.

C. Axial-angular pair correlations

So far we have shown our simulation results for the radial and axial structure of the colloidal suspension, characterized by the concentration profile $n(\rho)$ and the axial pair correlation function $g(z)$, respectively. The first one gives information on the local density of particles at a given distance from the center of the cylinder, whereas the second gives the probability of finding particles along the axis, at a given distance from a reference particle. As it was mentioned before, $g(z)$ does not take into account the displacement of the particles from the axis, neither $n(\rho)$ has information on the distribution of particles along z. To complete the picture, we have calculated the angular correlations between the particles, along the z axis. This has been made by computing the axial-angular correlation function $g(z,\varphi)$, defined in Sec. II. This function essentially measures the density of particles, from a reference particle, as a function of the axial distance and the angle.

First of all let us show how $g(z,\varphi)$ looks for a system where the z correlations are weak. For this we take the system defined by $R=30\sigma$ and $n_c^*=9\times10^{-4}$, whose axial pair correlation is plotted in Fig. 2(a). Figure 4 shows $g(z,\varphi)$ for this system. From this figure we see that this function is mainly a flat surface, with only small oscillations near the origin, which indicates that the correlations are rather weak both in the z and φ directions. The flatness of the surface comes from the fact that particles are allowed to move over a very wide region in the cylinder, as it is shown by its corresponding concentration profile, and thus, a particle has a large probability of finding particles at almost any distance and/or angle.

Let us mention that just like $g(z)$ in Figs. 2(a) and 2(b), the overall axial-angular correlation function $g(z,\varphi)$ in Fig.

4 is the result of the axial-angular correlations of the particles in each cylindrical shell corresponding to the various peaks of $n(\rho)$. Thus, it is interesting to consider the $g(z,\varphi)$ for each individual shell, which we also calculated. Also here, we found that the $g(z,\varphi)$ of the outermost shell strongly dominates the structure of the overall $g(z,\varphi)$. Thus, for example, for the outermost shell, $g(z=0,\varphi)$ exhibits the same sequence of maxima as observed in the overall $g(z=0,\varphi)$ in Fig. 4. The inner shells in contrast, exhibit a sequence with a smaller number of maxima. A simple semiquantitative explanation of the number of maxima in $g(z=0,\varphi)$ for each shell is the following:

If we carefully observe Fig. 4 for $z=0$, we see that there are 13 maxima. This indicates that, in addition to the particle located at $z=0$ (and $\varphi=0$), the probability to find another particle at the same axial position $z=0$ peaks at 13 evenly spaced angular locations. This feature is inherited directly from the $g(z,\varphi)$ of the outermost shell. For this shell, we can estimate by $2\pi\rho_1/l$ the number of particles that could be accommodated in a circle of diameter ρ_1 equal to the position of the outermost peak of $n(\rho)$, if they lied a distance $l=(n_c^*)^{-1/3}$ apart. From Fig. 1(a) for $n_c^*=9\times10^{-4}$, for example, we find that this number is approximately 12. This is an estimate of the minimum number of particles of the outermost shell that could coexist at the same axial position. As said above, our simulation of the $g(z,\varphi)$ for this shell leads to a number of 14 (including the reference particle at $\varphi=0$), i.e., 2 particles more than our estimate $2\pi\rho_1/l$. A similar estimate can be made for the inner shells, for which we also calculated $g(z,\varphi)$. For these, we also found that the number of maxima of $g(z=0,\varphi)$, plus the reference particle, exceeded our estimate by about 2. This then means that $g(z,\varphi)$ for the inner shells do differ from each other and from that of the outermost shell. However, the overall $g(z,\varphi)$ only reflects the main features of the latter. A similar scenario was also observed for $n_c^*=6\times10^{-4}$, and for the systems with $n_c^*=6\times10^{-4}$ and 9×10^{-4} for the smaller diameter $R=20\sigma$.

Still more interesting is the case when the suspension is highly confined, as in Figs. 1(c) and 2(c). In those cases we found that the highly restricted space in which the particles were confined had very important effects on the radial and axial structure of the suspension, and something similar is expected to happen for the angular correlations.

Figure 5(a) illustrates the behavior of the axial-angular pair correlation function $g(z,\varphi)$ for the system defined by $R=10\sigma$ and $n_c^*=3\times10^{-4}$. Here we see a rather different qualitative and quantitative behavior than in the case presented just above. This surface is not flat anymore. Instead, it presents strong oscillations along the z axis, which indicates that the particles are highly correlated along this coordinate, a feature already pointed out when discussed the axial correlations corresponding to this system. On the other hand, the surface does not have oscillations along the φ axis, which indicates that the particles are still angularly uncorrelated. Recalling that in fact the particles are confined into a very narrow region at the center of the cylinder and that they are widely spaced in the z direction, it is not surprising that the particles are able to sample all the values of φ with equal probability.

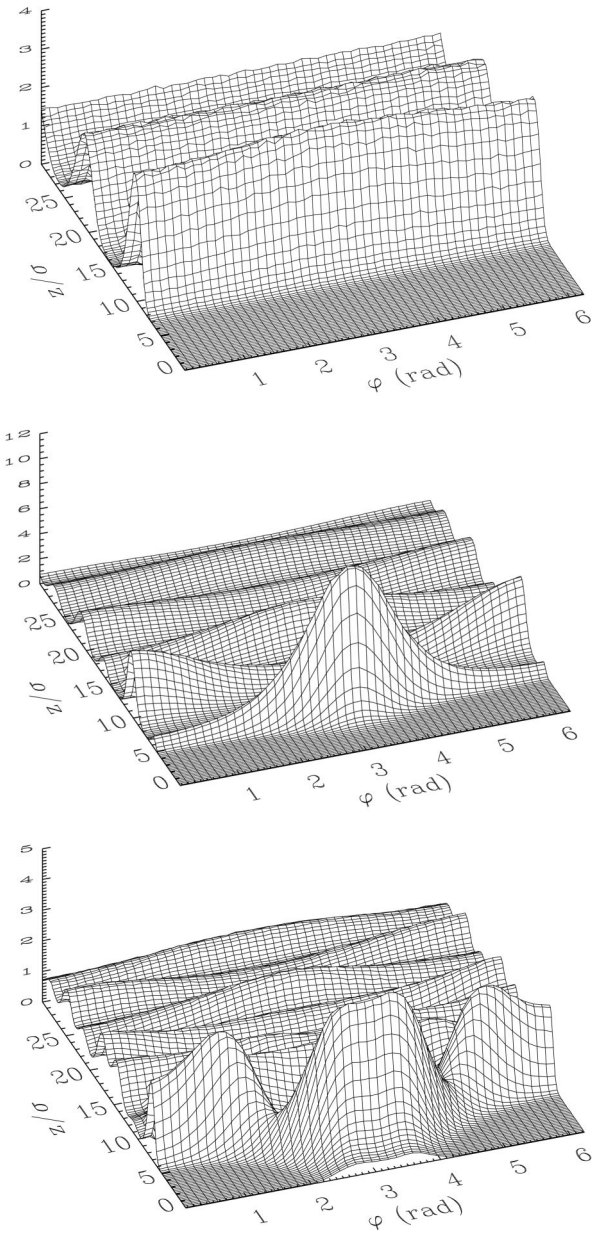

FIG. 5. Axial-angular pair correlation function for different densities and for $R=10\sigma$. (a) Upper figure: $n_c^*=3\times10^{-4}$; (b) middle figure: $n_c^*=6\times10^{-4}$; (c) lower figure: $n_c^*=9\times10^{-4}$. The other parameters are $A_p=400$, $A_w=400$, and $z_D=0.15$.

However, one should expect that the particles become correlated on the angular direction as a result of stronger interactions between the particles when the density increases. This is illustrated in Fig. 5(b) for the system with density $n_c^*=6\times10^{-4}$. In this figure we see that a well defined, single peak has appeared in the surface. Such a peak, although broad, has its maximum at $\varphi=\pi$. Beyond this peak, in the z direction, we see another broader peak at $\varphi=2\pi\equiv0$, then another at $\varphi=\pi$ and so on. Notice that the height of these peaks, i.e., the angular correlations, weaken rather rapidly with the axial distance. The interpretation of such peaks is as follows: standing on the reference particle, and facing the center of the cylinder, the first peak indicates that the first neighbors (along the z axis) are mainly located just in front of the particle ($\varphi=\pi$), the second neighbors are

located just above the central particle ($\varphi=0$), the third neighbors are in front, and so on. This pattern clearly indicates that particles arrange themselves into a structure that looks very similar to a zig-zag, as seeing from the central particle. In some sense, this process, in which the system goes from a state in which the particles are basically confined into a line, to a state in which the structure brakes into a zig-zag, i.e., into a two-line structure, resembles a buckling transition, although in this case the transition is observed at the level of the pair correlations.

It is interesting to notice that such a transition only increases a little the region occupied by the particles in the ρ direction, but compresses the structure importantly in the z direction, as the comparison between the corresponding concentration profiles and axial correlations in Figs. 1(c) and 2(c) indicates. This means that up to these densities, the radial structure is mainly dominated by the repulsive interaction exerted by the wall. Beyond a certain threshold density, the interaction between the particles becomes so strong that the particles have to leave the center of the cylinder, producing the shell of particles shown in Fig. 1(c) for the case $n_c^*=9\times10^{-4}$. In Fig. 5(c) we plot the corresponding $g(z,\varphi)$ for this system. Although one can clearly appreciate the strong angular correlations among the particles, this figure does not show well defined peaks as in the previous system. In fact, the axial correlations for this case [see Fig. 2(c) for $n_c^*=9\times10^{-4}$] have an anomalous behavior in the sense that, unlike a typical pair correlation function, the second peak is higher that the first, the third is higher than the fourth, etc. This behavior might indicate that the system is undergoing a structural transition, since by further increasing the density, the system changes to a structure in which a well defined sequence of peaks appear, corresponding to the next expected structure. Figure 6(a) illustrates this for a system with $n_c^*=11\times10^{-4}$. If we still increase further the density, as illustrated in Fig. 6(b), it is possible to get even a periodic array of peaks, i.e., a structure whose angular correlations become of very long range, indicating that the system is close to form an ordered array on a cylindrical surface (or better said, on a cylindrical shell) since for this value of the density ($n_c^*=17\times10^{-4}$), the density profile $n(\rho)$ still exhibits only a single peak. Although not shown here, this periodic array on a cylindrical shell is not the final state of the system since under further increasing the density of particles, the radial structure evolves from the single-peak concentration profile to a two-peak concentration profile, very similar to the curve illustrated in Fig. 1(b) for the case $n_c^*=9\times10^{-4}$ and $R=20\sigma$.

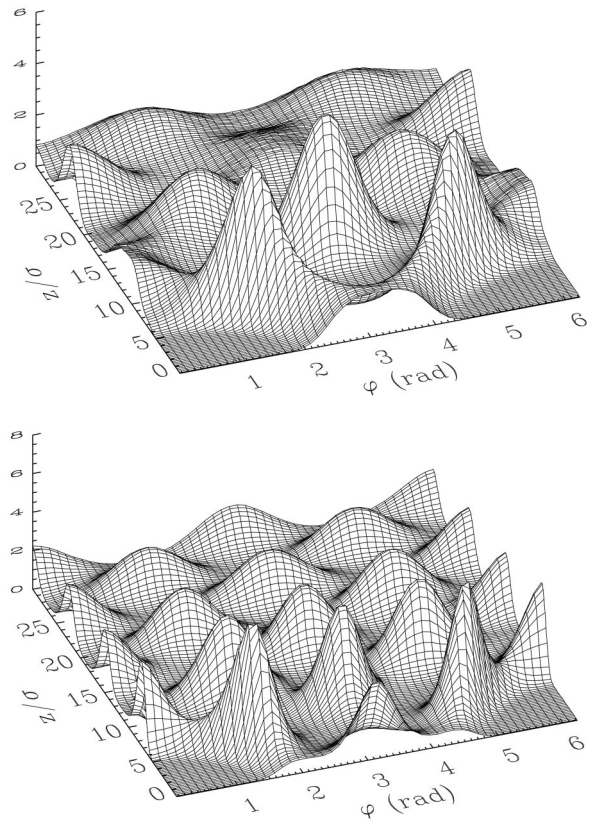

FIG. 6. Axial-angular pair correlation functions for the same parameters as in the previous figure and for two different densities. (a) Upper figure: $n_c^*=11\times10^{-4}$; (b) lower figure: $n_c^*=17\times10^{-4}$.

IV. SUMMARY

In this work we have presented a Monte Carlo study of the structure of a model colloidal suspension confined in a cylindrical pore. The interaction between the particles was assumed to be the repulsive part of the DLVO potential, i.e., a hard sphere plus a Yukawa potential, and the corresponding choice was made for the wall-particle interaction. The structure of the suspension, on the other hand, has been described through the local concentration profile and through contracted versions of the inhomogeneous pair correlation function between the particles. These correlations functions allowed us to illustrate the ordering developed by these systems under conditions of strong confinement.

The structure of the suspension was studied as a function of the concentration of particles and the size of the pore, and depending on the combination of the parameters defining the system a variety of structures were observed. For the concentration profile, we found that the suspension evolves from a layered structure in which the particles occupy most of the available radial space in the cylinder, up to a structure in which the particles are completely confined to the center of the cylinder. In this process, the system adopts structures in which, for instance, the particles are restricted to move in a cylindrical shell, or also disconnected structures in which one part of the suspension is confined to the cylinder axis, whereas another part is confined to a cylindrical shell. The appearance of such structures has been associated to the competition between the repulsive interaction between the particles, and the confining interaction exerted by the wall.

As for the correlations between the particles, in this work we have defined two quantities that give information on the relative ordering between the particles, namely, the axial pair correlation function, $g(z)$, and the angular correlation function, $g(z,\varphi)$. Through these functions we have shown that, under severe confinement, the system develops a well-defined axial and angular ordering. Thus, we have shown that for very low concentrations the particles form a 1D structure where there are clear and strong axial correlations, but the angular correlations are absent. For larger values of the concentration of particles in the cylinder, the axial struc-

ture weakens and the particles develop well defined angular correlations, in such a way that the structure of the suspension goes from a state in which all the particles are aligned along the *z* axis, to a state in which the linear structure breaks into a zig-zag. For larger values of the concentration we found that the angular correlations become longer ranged, and the particles practically form an ordered array on a cylindrical shell. In spite of this angular ordering, we have shown that the axial correlations are dominated by the 1D character of the system when the suspension is strongly confined.

ACKNOWLEDGMENTS

This work was supported by the Consejo Nacional de Ciencia y Tecnología (CONACyT, México) through Grant No. 3882E and through financial support to M.C.-P., and by the Programa de Simulación Molecular del Instituto Mexicano del Petróleo (IMP, México). M.M.-N. acknowledges the kind hospitality and support of the Institute of Theoretical Physics of the University of California at Santa Barbara. We also thank the Computer Center of the Universidad de Guadalajara, México, where some calculations were made.

[1] R. Evans, Adv. Phys. **28**, 143 (1979).

[2] P. Gozález-Mozuelos, J. Alejandre, and M. Medina-Noyola, J. Chem. Phys. **95**, 8337 (1991); **97**, 8712 (1992); P. González-Mozuelos, *ibid.* **98**, 5747 (1993); P. González-Mozuelos and J. Alejandre, *ibid.* **105**, 5949 (1996).

[3] M.D. Carbajal-Tinoco, F. Castro-Román, and J.L. Arauz-Lara, Phys. Rev. E **53**, 3745 (1996); G.M. Kepler and S. Fraden, Phys. Rev. Lett. **73**, 356 (1994); J.C. Crocker and D.G. Grier, *ibid.* **73**, 352 (1994); D.H. van Winkle and C.A. Murray, Phys. Rev. A **34**, 562 (1986); D.H. van Winkle and C.A. Murray, J. Chem. Phys. **89**, 3885 (1988).

[4] E.W.J. Verwey and J.T.G. Overbeek, *Theory of the Stability of Lyophobic Colloids* (Elsevier, Amsterdam, 1948).

[5] M. Meina-Noyola and D.A. McQuarrie, J. Chem. Phys. **73**, 6279 (1980).

[6] M. Chávez-Páez, H. Acuña-Campa, L. Yeomans-Reyna, M. Valdez-Covarrubias, and M. Medina-Noyola, Phys. Rev. E **55**, 4406 (1997).

[7] M. Chávez-Páez, E. Urritua-Bañuelos, and M. Medina-Noyola, Phys. Rev. E **58**, 681 (1998).

[8] M. P. Allen and D. J. Tildesley, *Computer Simulation of Liquids* (Clarendon Press, Oxford, 1987).

[9] D. A. McQuarrie, *Statistical Mechanics* (Harper and Row, New York, 1975).